Nuclear Physics **A496** (1989) 205-223
North-Holland, Amsterdam

ELASTIC SCATTERING OF POLARIZED PROTONS BY ^{6}Li* (II). Phase-shift analysis

M. HALLER, W. KRETSCHMER, A. RAUSCHER, R. SCHMITT[1] and W. SCHUSTER

Tandemlabor der Universität Erlangen-Nürnberg, Erlangen, Fed. Rep. Germany

Received 9 August 1988
(Revised 20 December 1988)

Abstract: For a test of recent resonating-group calculations of ^{7}Be the elastic-scattering data for ^{6}Li(p, p_0), described in the preceding paper, were analyzed with the phase-shift method. Both differential cross section and analyzing power are well described over the whole energy range of 1.6 MeV $\leq E_p$(lab) $\leq$ 10 MeV. From the energy behaviour of the complex scattering phase shifts four broad overlapping resonance structures with total angular momentum $\frac{1}{2}$, $\frac{3}{2}$, $\frac{5}{2}$ and negative parity have been deduced. These resonances, located at excitation energies in ^{7}Be between 9 and 13 MeV have not been observed before, but have been predicted by the above mentioned calculations. The predicted resonance behaviour of the $^2P_{3/2}$ phase shift was not confirmed by our analysis. Additionally a direct comparison of the data with the predictions of different resonating-group calculations is shown for some selected energies.

E NUCLEAR REACTIONS ^{6}Li(polarized p, p), E = 1.6-10 MeV; measured $\sigma(E, \theta)$, $A(E, \theta)$, ^{6}Li(polarized p, p')^{6}Li*; E = 5.9 MeV; measured $\sigma(\theta)$, $A(\theta)$. ^{7}Be deduced resonances, Γ, Γ_p, J, π.

1. Introduction

Recently, the $A = 7$ nuclear systems were investigated by the refined multichannel and multistructure resonating-group method [1]). Several new levels in ^{7}Be are predicted [2]) by these calculations, which are sketched on the level schemes in fig. 1. According to the assumption in the theoretical calculations each of them has an isospin $T = \frac{1}{2}$. Most of these levels in the excitation energy region 6 MeV $\leq E_x \leq$ 11 MeV are expected to appear as resonances in the elastic ^{6}Li(p, p) scattering (E_p(lab) < 10 MeV) with the corresponding J^π values of $\frac{1}{2}^-$, $\frac{3}{2}^-$, and $\frac{5}{2}^-$. The predicted $J^\pi = \frac{7}{2}^-$ levels, however, are suppressed in this energy range by the large angular momentum barrier.

As the existing polarized data [3]) are restricted to energies below 3.2 MeV, we measured full angular distributions of differential cross sections σ and analyzing power A in small energy steps from 1.6 MeV (σ) and 2.8 MeV (A) to 10 MeV laboratory energy. The details of the experiment are discussed in the preceding paper.

* Supported by the Deutsche Forschungsgemeinschaft.

[1] Present address: FAG Kugelfischer, Erlangen, Fed. Rep. Germany.

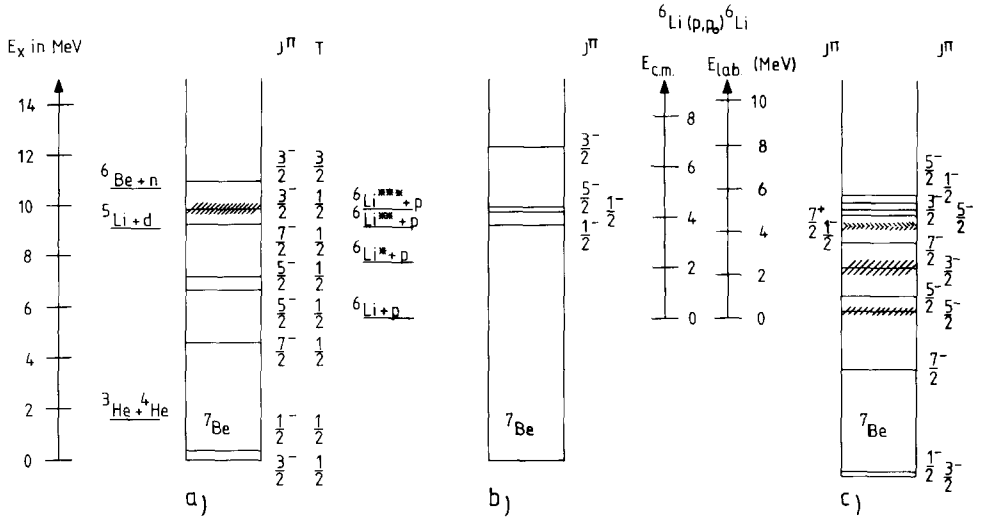

Fig. 1. Level-scheme of ^{7}Be with the results of the present work (b), compared with an experimental scheme of ref. [15]) (a), and with the prediction of the refined resonating-group model (c).

Unpolarized cross sections of ^{6}Li(p, p) elastic scattering have already been measured by Harrison and Whitehead [4]). The excitation functions reveal a broad resonance structure at $E_p \approx 5$ MeV, which is confirmed by our data (see the preceding paper). It proved impossible, however, to carry out an unambiguous analysis of this structure without including analyzing power data, because the parameter space of the contributing phase shifts is too large. This is due to the complicated spin configuration of the p+^{6}Li system.

2. Phase-shift parameters

The spin-1 target nucleus ^{6}Li and the spin-$\frac{1}{2}$ projectile yield the possible channel spins $S = \frac{1}{2}$ (doublet) and $S = \frac{3}{2}$ (quartet). Coupling channel spin and orbital angular momentum L yields the total angular momentum J; the notation is $^{2S+1}L_J$. The possible configurations for $L = 0, 1$, and 2 are sketched in fig. 2. Whereas J and parity π are good quantum numbers, mixing of states with different S and/or L values is possible by noncentral components of the nucleon–nucleon-interaction force. The corresponding mixing-parameters are written here in the notation $S_{J\pi}$, $L_{J\pi}$ and $LS_{J\pi}$: S denotes channel-spin mixing, L orbital angular-momentum mixing, and LS both. The unique J and π values of the two mixing states are added as indices (see fig. 2).

In this work the scattering matrix (S-matrix) is parametrized according to Seyler [5]), whose spin-1 + $\frac{1}{2}$ parametrization is a generalized Blatt–Biedenharn [6]) method. In contrast to the complex eigenphase shifts, the mixing-parameters are assumed to be real. In this way difficulties are avoided, which arise from hermiticity requirements

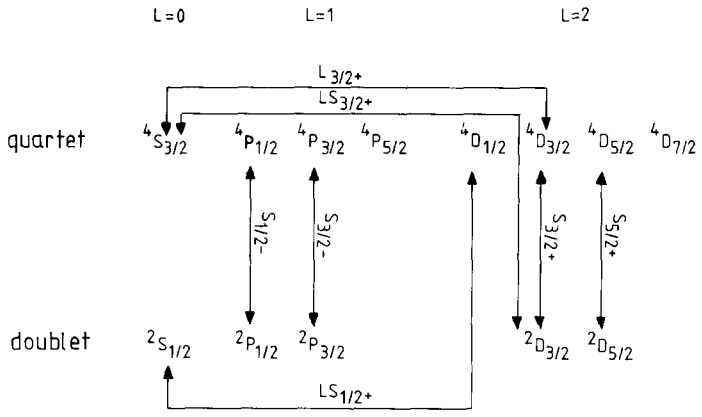

Fig. 2. Phase-shift and mixing-parameters for the spin-$\frac{1}{2}$ at 1 scattering phase-shift analyses, including angular momenta up to $L = 2$.

of the S-matrix [5]). Nevertheless, the parameter space is very large due to 13 complex eigenphase shifts ($L = 0, 1, 2$) and 7 real mixing-parameters ($J = \frac{1}{2}, \frac{3}{2}, \frac{5}{2}$). Angular momenta larger than 2, however, proved to be negligible. Even the D-phase shifts were generally small, and their imaginary parts could be set zero. The mixing-parameters, however, could not be neglected, because they influenced the observables significantly, mainly the analyzing power. Good descriptions of the data were achieved only by adjusting them like free fit parameters. This means, that tensor-force effects have to be taken into account. In the resonating-group model calculations of ref. [1,2]), this modified Blatt-Biedenharn parametrization was not applied, but the S-matrix elements themselves were used instead. The mixing-parameters used there are also important, yet they do not correspond to the mixing-parameters of the present work.

3. Procedures of the phase-shift analysis

The phase-shift calculations were carried out using the computer code HALFONE from the ETH Zürich. Formerly, it had been used by Jenny for analyzing ^{3}He(d, d) scattering [7]) and by Schmelzbach *et al.* for investigations of the proton-deuteron scattering [8]).

The fitting algorithm minimizes the χ^2 type error function

$$\chi^2_e = \sum_{i=1}^{N} \left(\frac{x_i - y_i}{\Delta x_i} \right)^2 .$$

Here x_i denotes the ith experimental value with error $\pm\Delta x_i$, and y_i denotes the corresponding calculated value. In the procedures of this section each fit includes the data of one energy, using the results as starting values for the subsequent fit of

the data at the adjacent energy. Since there are too many parameters for simultaneous variation, they are divided into two groups: S- and P-phases in one group, D-phases and mixing-parameters in the other. They were varied alternatingly keeping the other group of parameters fixed. Predictions of recent resonating-group calculations [9]) were taken as guidelines for proper starting values of the eigenphase-shifts. In this way, good descriptions of the data are achieved. In fig. 3 the resulting phase shifts are displayed in so-called Argand plots, where x- and y-axis represent the real and imaginary part of $\exp(2i\delta(E))$, respectively. Here $\delta(E)$ denotes the eigenphase shift as function of the c.m. energy E. As can be seen from fig. 3, there are 4 phase shifts which show resonance structures in their Argand plot:

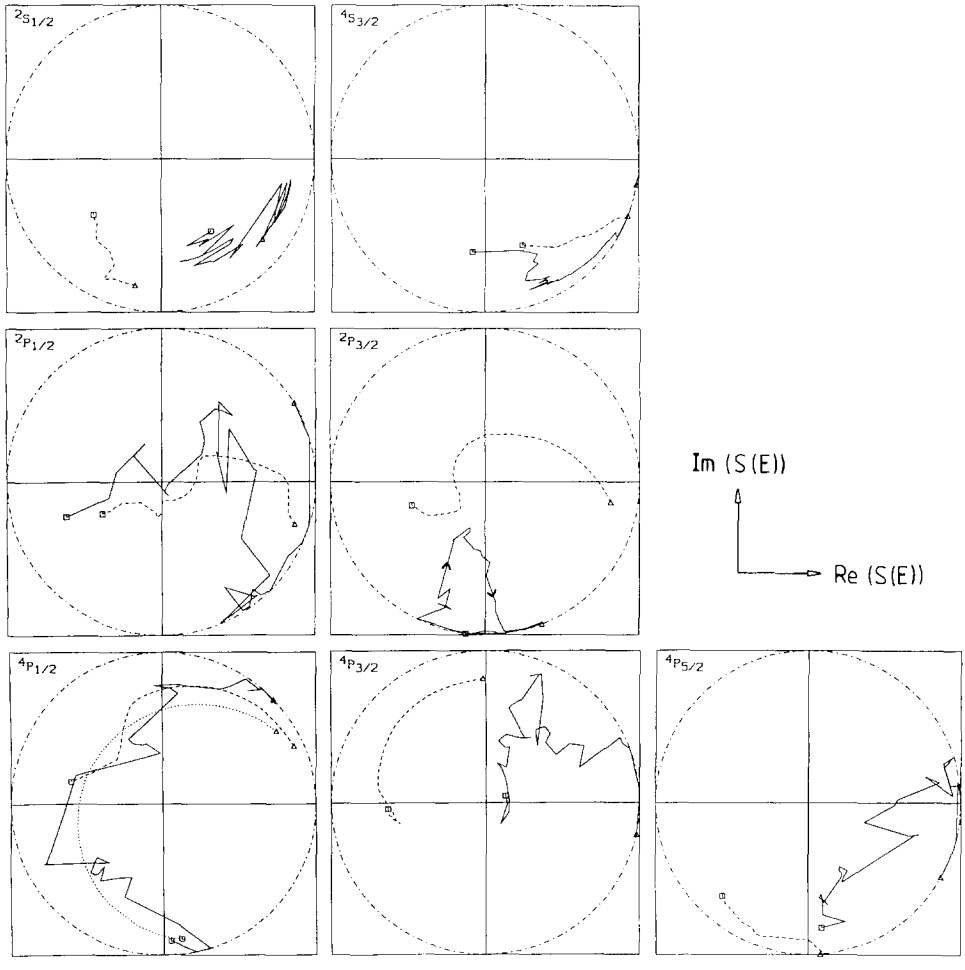

Fig. 3. Argand plots for the S and P phase shifts with all parameters adjusted (see text), compared with the predictions of ref. [9]) (dashed curves) ($\triangle E_{lab} = 2.8$ MeV, $\square E_{lab} = 10$ MeV). The Breit-Wigner parametrization curve for the $^4P_{1/2}$ phase shift is drawn as a dotted curve.

$^2P_{1/2}$, $^4P_{1/2}$, $^4P_{3/2}$, and $^4P_{5/2}$. The corresponding predictions of the resonating-group model [9]) are quite similar. The structure of the $^2P_{3/2}$ phase shift, however, is no evidence for a resonance, because it rotates clockwise. More quantitative descriptions of the resonances were achieved by a Breit-Wigner parametrization [10]) of the resonant S-matrix elements

$$S(E) = e^{2i\delta(E)} = e^{2i\lambda(E)}\left[e^{-2\mu(E)} + \frac{i\Gamma_p}{E_R - E - \frac{1}{2}i\Gamma}\right].$$

In this way, the resonance is described by the total width Γ, the partial width Γ_p and the resonance energy E_R. The potential scattering background phase shift is $\lambda + i\mu$, while the resonance mixing phase is neglected to keep the number of free parameters small.

The vectors from the Argand-plot coordinates to the corresponding (i.e. equal energy) points on the parametrization curve are plotted in fig. 4. Minimization of the square sum of the absolute values of these vectors is performed by varying the resonance parameters and the coefficients of the background phase shifts via the ansatz

$$\lambda = c_\lambda E, \qquad \mu = c_\mu E^2 \quad (c_\mu \geq 0).$$

In this way, resonance structures were obtained which were fixed in subsequent phase-shift calculations to fit the data. Proceeding from one resonant phase-shift to the other, the number of free phase-shift parameters was reduced by 2 in each step.

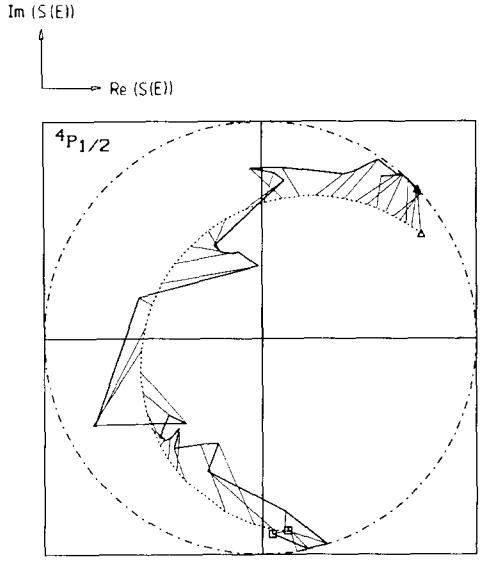

Fig. 4. Description of the experimental Argand plot by the optimized parametrization curve (e.g. $^4P_{1/2}$ phase shift).

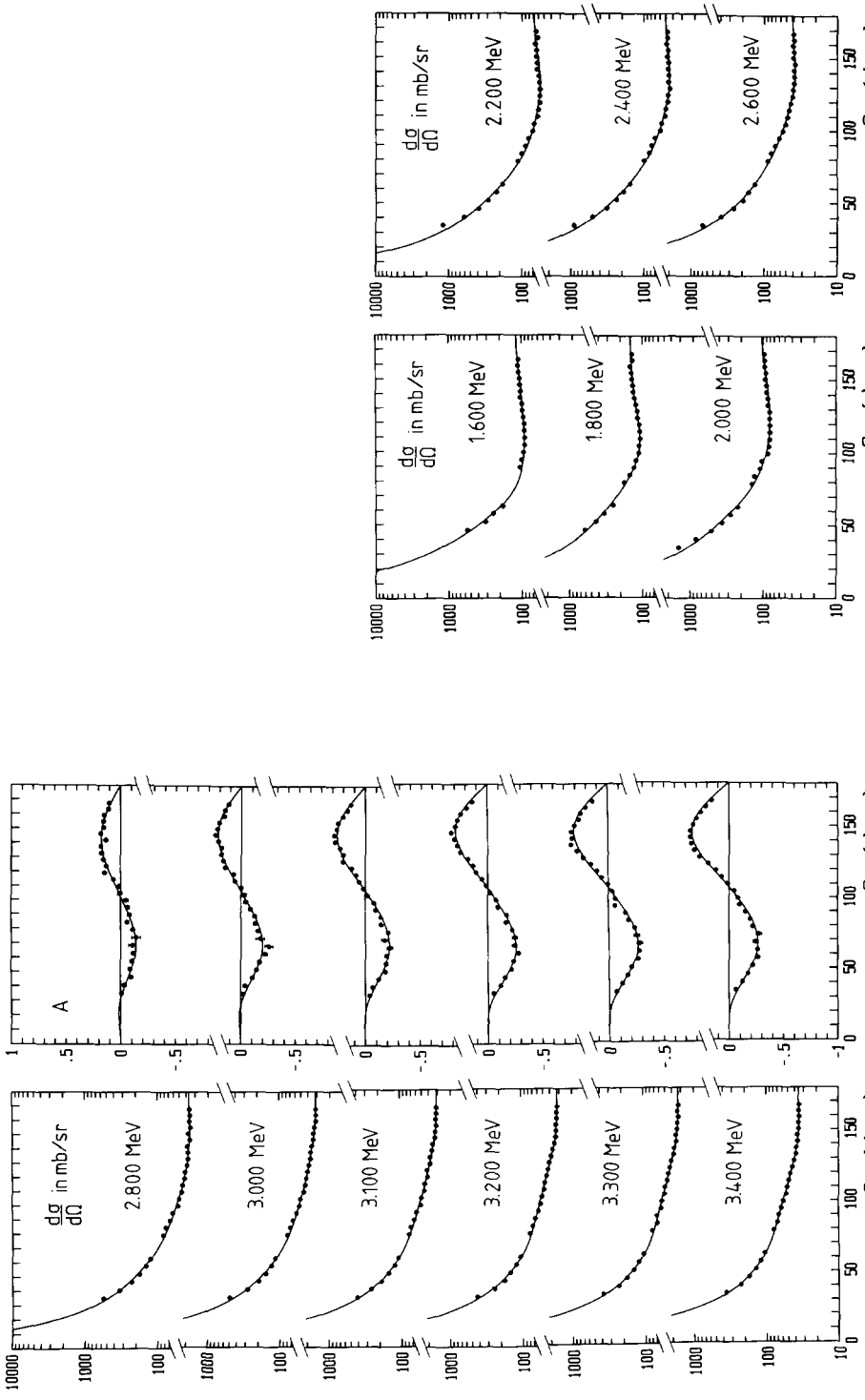

Fig. 5. Differential cross section and analyzing-power data, compared with phase-shift calculations (see text). The energies are given in the laboratory system.

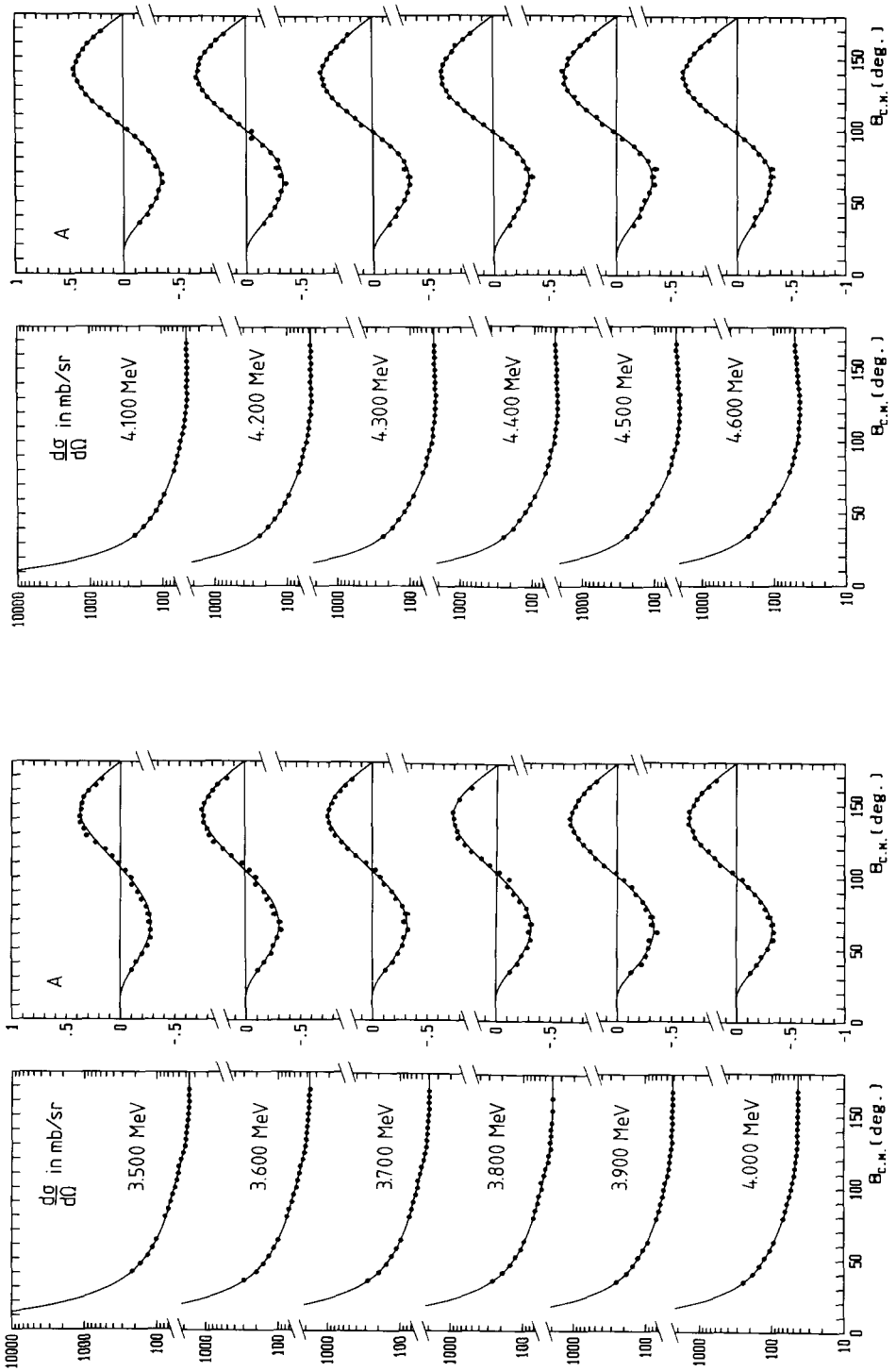

Fig. 5—continued

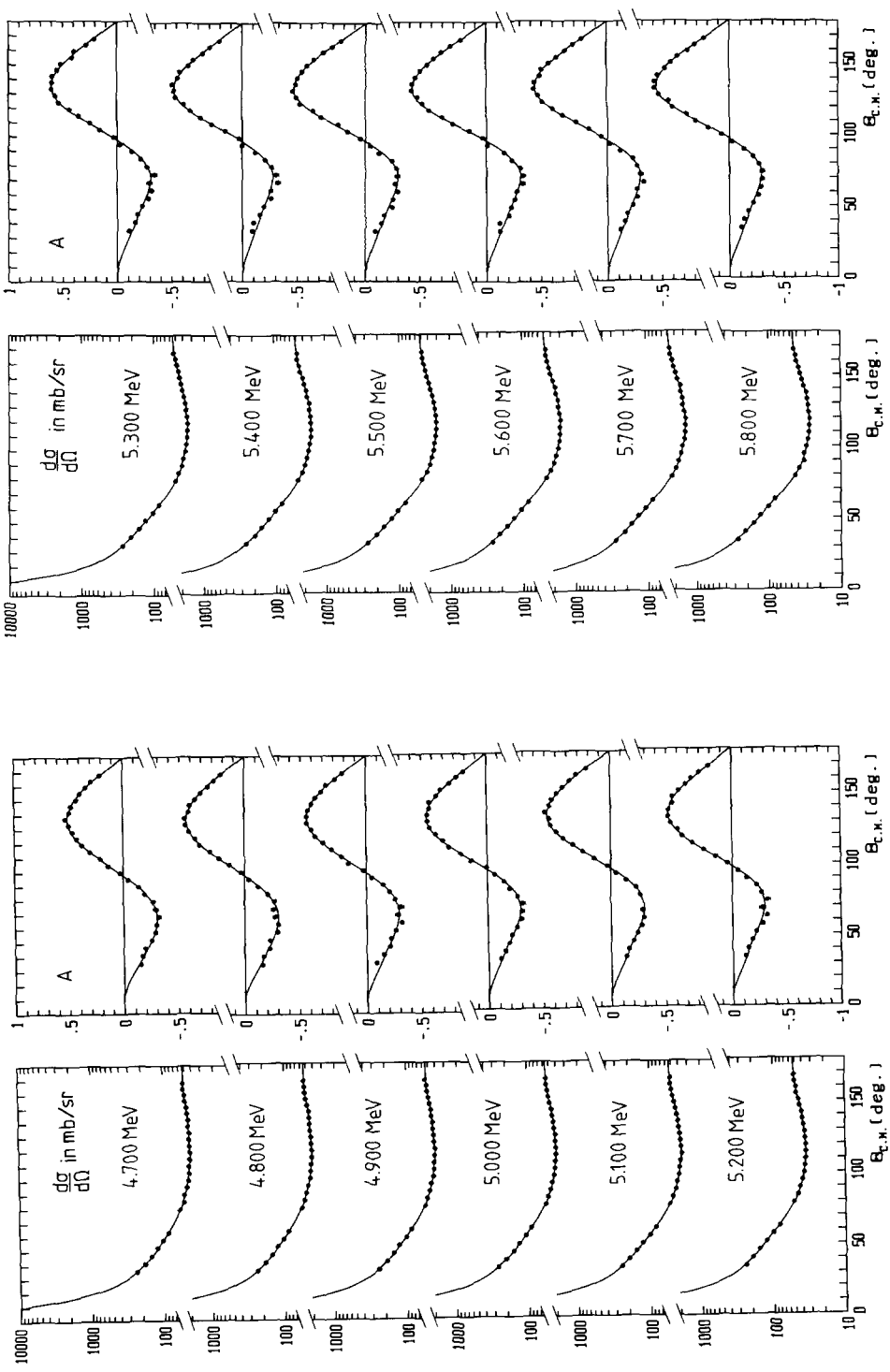

Fig. 5—continued

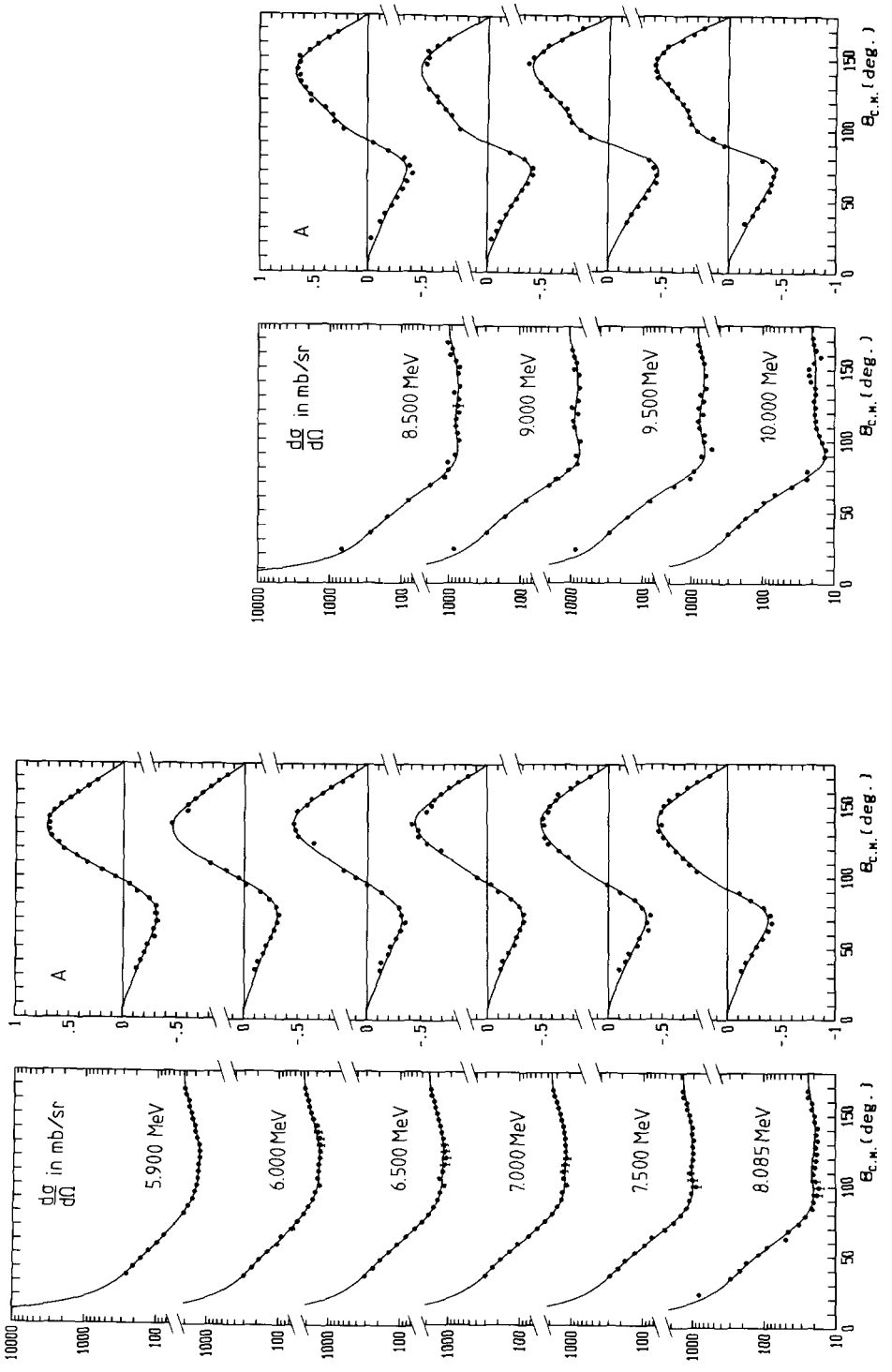

Fig. 5—continued

Finally, the 4 resonant phase shifts $^2P_{1/2}$, $^4P_{1/2}$, $^4P_{3/2}$, and $^4P_{5/2}$ were parametrized according to the Breit-Wigner-formula, only the remaining parameters being directly adjusted to fit the data. The description of the data (see fig. 5) was nearly as good as in the first analysis, in which all parameters were varied.

The resulting Argand plots are shown in fig. 6. In the case of the $^2P_{1/2}$ and the $^4P_{1/2}$ phase shifts there is good agreement with the predictions of the resonating-group calculations, whereas there is some offset in the case of the $^4P_{3/2}$. There is no prediction of the $^4P_{5/2}$ resonance structure in the energy range of interest. The rotation of the $^2P_{3/2}$ phase shift was clockwise in each calculation which is in contradiction to the theoretical prediction with a resulting resonance structure.

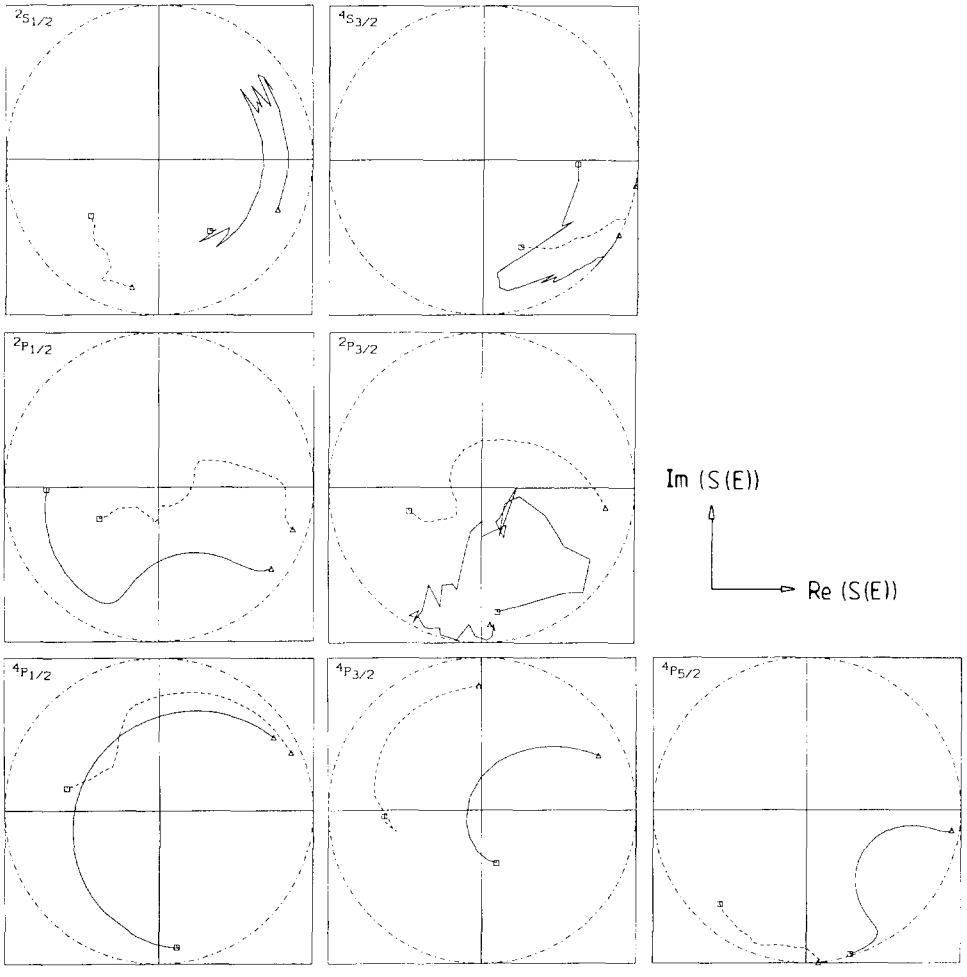

Fig. 6. Argand plots, corresponding to the calculations of fig. 5. The resonant phase shifts are parametrized by a Breit-Wigner formula (see text) ($\triangle$-E_{lab} = 2.8 MeV, $\square$-E_{lab} = 10 MeV). The dashed curves refer to the predictions of ref. [2]).

TABLE 1

Resonance parameters and background phase-shift coefficients resulting from the procedure described in sect. 3. The energies are given in the c.m. system; E_x denotes the excitation energy relative to the ^{7}Be ground state

Phase shift	E_x (MeV)	E_R (MeV)	Γ_p (MeV)	Γ (MeV)	C_λ (MeV^{-1})	C_μ (MeV^{-2})
$^4P_{1/2}$	9.80	4.19	1.68	2.23	−0.0599	6.20×10^{-4}
$^4P_{3/2}$	12.34	6.73	1.77	4.74	0.0124	4.86×10^{-3}
$^4P_{5/2}$	9.95	4.34	0.40	1.47	−0.0693	4.05×10^{-6}
$^2P_{1/2}$	9.29	3.68	0.32	1.28	−0.177	2.11×10^{-3}

In table 1 the resonance parameters and background phase-shift coefficients are listed. The resonance energies can also be seen in fig. 7, where the real parts of the S and P phase shifts are compared with the theoretical predictions.

At 1.57 MeV c.m. energy (i.e. 1.84 MeV in the laboratory system), there appears a further $\frac{5}{2}^-$ resonance, which has been analyzed by McCray [11]) in a study of the unpolarized cross section. His results were $\Gamma_p = 0.798$ MeV and $\Gamma = 0.836$ MeV. To carry out a phase shift analysis it is essential, however, to include analyzing power data. Since our polarization data start at 2.8 MeV laboratory energy, we included the analyzing power data of Petitjean *et al.* [12]) in the energy range from 1.6 to 2.6 MeV to our analysis. Due to the only slightly structured angular distributions and the few amount of data points, compared with the large number of contributing phase shifts, there are still ambiguities in the phase shift analysis. Proceeding from 2.8 to 1.6 MeV in steps of 0.2 MeV laboratory energy, the cross section and analyzing-power data were fitted similarly to the procedure described at the beginning of this section. The D coupling phase shifts, however, were set zero to reduce the number of parameters. The $^4P_{5/2}$ phase shift was not varied, but calculated according to the Breit–Wigner formula, using the resonance parameters of McCray [11]). In this way, a good description of the data was achieved, as can be seen in fig. 8. The varied S and P phase shifts, as well as the P coupling phase shifts, nearly smoothly follow the trend of the higher-energy behaviour. This result may confirm the supposed $\frac{5}{2}^-$ value as well as the resonance parameters of ref. [11]). To remove the ambiguities in the phase-shift analysis, more analyzing-power data in small energy steps and full angular distributions should be measured in the range below 2.8 MeV proton energy.

4. Simultaneous description of all data with energy-dependent phase-shift parameters

In the previously discussed calculations for energies above 2.8 MeV, the resonance parameters were determined by Breit–Wigner parametrization of the resonance structures. To test for mutual interdependence of overlapping resonances, and to estimate the errors, in a second approach all experimental data between 2.8 and 10 MeV were fitted simultaneously. In this procedure, the energy dependence of the

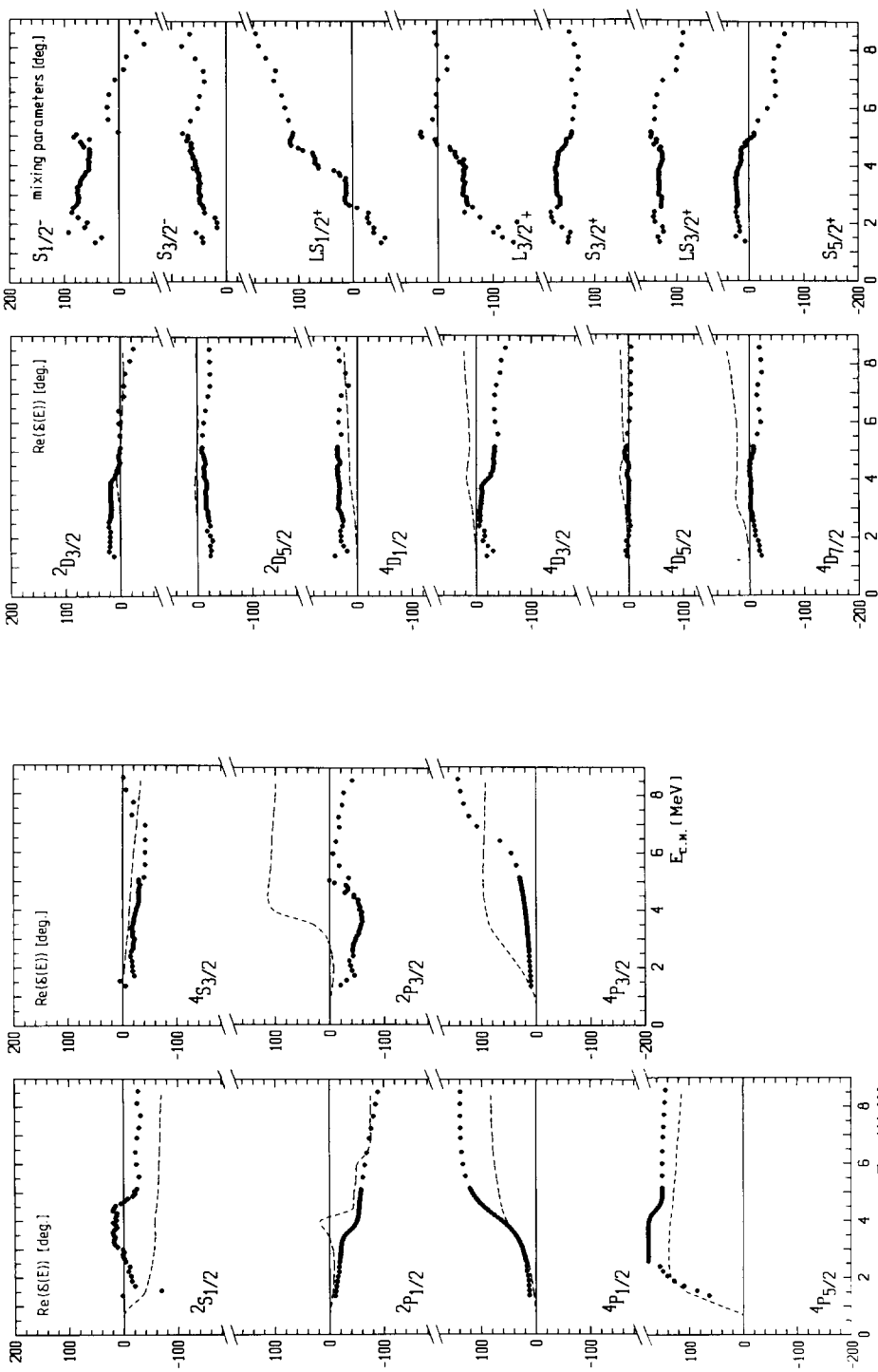

Fig. 7. Real parts of the S and P phase shifts, D phase shifts and mixing-parameters corresponding to the calculation shown in figs. 5 and 6. Predictions of ref. [2]) are plotted as dashed curves. $^4P_{5/2}$ values below 3 MeV correspond to the analysis described at the end of sect. 3, using the resonance parameters of McCray [11]).

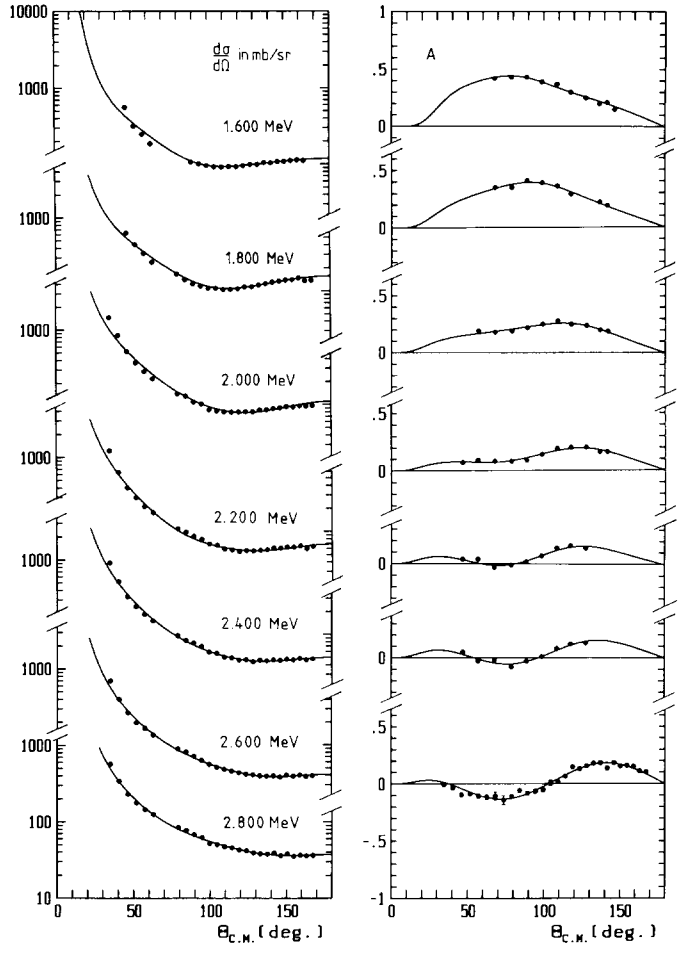

Fig. 8. Phase-shift calculations for laboratory energies from 1.6 to 2.8 MeV, using the $\frac{5}{2}^-$ resonance parameters of McCray [11]). The analyzing-power data are adopted from Petitjean *et al.* [12]).

TABLE 2

Resonance parameters and reduced widths, resulting from the procedure described in sect. 4. The energies are given in the c.m. system; E_x denotes the excitation energy relative to the ^{7}Be ground state. The errors refer to a 10% increase of the χ^2 function, averaged over all energies

Phase shift	E_x (MeV)	E_R (MeV)	Γ_p (MeV)	Γ (MeV)	γ^2 (MeV)
$^4P_{1/2}$	9.81 ± 0.12	4.20 ± 0.12	1.65 ± 0.25	2.21 ± 0.29	0.57 ± 0.086
$^4P_{3/2}$	12.37 ± 1.27	6.76 ± 1.27	1.81 ± 1.03	4.95 ± 3.23	0.47 ± 0.267
$^4P_{5/2}$	10.00 ± 0.17	4.39 ± 0.17	0.42 ± 0.14	1.68 ± 0.58	0.14 ± 0.047
$^2P_{1/2}$	9.29 ± 0.31	3.68 ± 0.31	0.47 ± 0.33	1.93 ± 0.96	0.18 ± 0.126

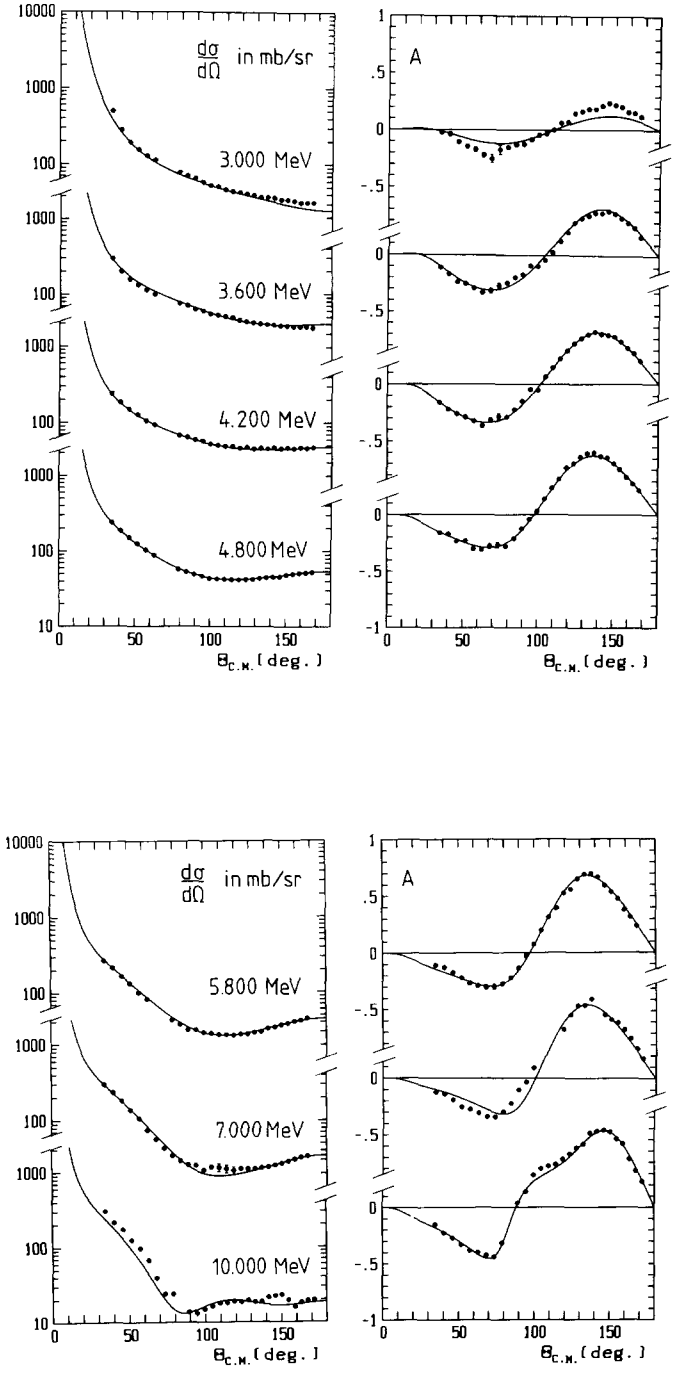

Fig. 9. Description of the data by a phase-shift calculation which fits all data simultaneously using energy-dependent parameters, for some sample energies (laboratory system).

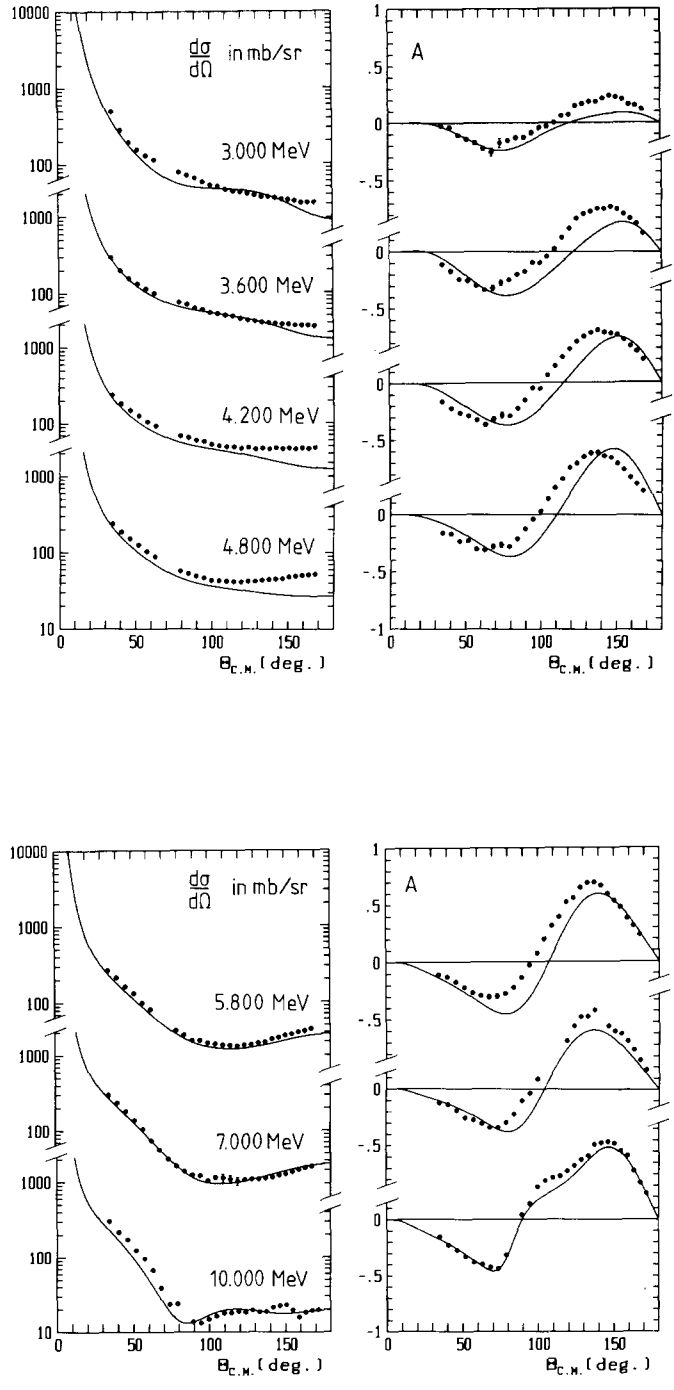

Fig. 10. Phase-shift calculations similar to fig. 9, the $^4P_{1/2}$ resonance being "switched off".

nonresonant phase shifts and the mixing-parameters is described by third-order polynomials, the coefficients being adjusted to the data. The resonant phase shifts were again described by a Breit-Wigner formula. The error function in this new fit procedure was calculated from the χ^2_e values (see sect. 3) achieved for each energy.

$$F_{\text{total}} = \sum_{\text{energies}} \frac{\chi^2_e}{\chi^2_{e,\text{best}}}.$$

The $\chi^2_{e,\text{best}}$ means the corresponding error function value for the single-energy best fit (sect. 3). In this way, the number of parameters was reduced drastically to 129 parameters (resonance parameters and polynomial coefficients) for about 2160 data points, in contrast to 27 parameters for about 54 data points in the case of the single-energy fits. On the other hand, the necessary amount of computer time was comparatively large. It was not feasible to vary all parameters simultaneously; therefore they were divided into three groups, which were varied alternatingly. After adjusting the non-resonant phase shifts, the resonance parameters were varied, too. The resulting values (see table 2) did not much differ from the values obtained in the procedure of sect. 3, although in the present procedure interdependences of different, overlapping resonances may occur. The errors listed in table 2 refer to an increase of the total error function F_{total} by 10%, which corresponds to a relatively poor description of the data on resonance compared to the situation at distant energies. The description of the data is shown for some energies in fig. 9. The Argand plots are quite similar to those obtained by the single energy fits (sect. 3).

The sensitivity of the observables to one single resonance can be seen for instance in fig. 10, where the $^4P_{1/2}$ resonance is omitted in the calculation. Apparently the analyzing power is much more sensitive than the unpolarized cross section.

5. Comparison of the data with resonating-group predictions

In fig. 11a, analyzing-power data of this work and neutron scattering data [13]) at $E_p = 10$ MeV are compared with the corresponding predictions [9]), where compared to the earlier calculations of ref. [2]), more structures and more channels were taken into account. Proton and neutron scattering data nearly coincide, whereas in both cases there are some discrepancies to the predictions in the backward angular region. This has been improved by slightly modified calculations [14,9]), in which the root mean square radius of the ^{6}Li nucleus was updated according to the experimental value (see the dot-dashed curve in fig. 11b). The overall shapes of the experimental angular distributions agree reasonably well even with the earlier resonating-group calculations of ref. [2]), as can be seen for some examples in fig. 12. The predictions for the analyzing power change significantly, if the $\frac{7}{2}^+$ channel is omitted in the calculations. In fig. 13, the observables for the inelastic scattering ^{6}Li(p, p)^{6}Li* (E_x = 2.183 MeV) at 5.9 MeV proton energy, are compared with resonating-group calculations [2]) and with unpolarized neutron scattering data of ref. [15]), quoted in ref. [2]).

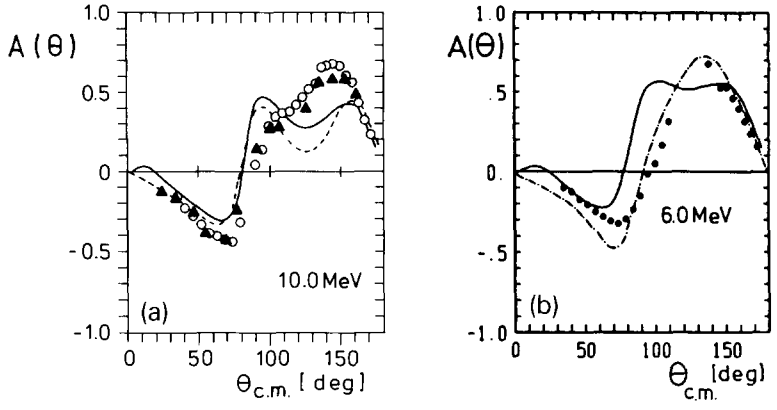

Fig. 11. (a) Analyzing-power data of elastic 10 MeV proton (○) and neutron [13]) (▲) scattering at ^{6}Li, compared with corresponding resonating-group predictions [9]) for p (solid curve) and n (dashed curve). (b) Analyzing-power data of elastic 6 MeV proton scattering, compared with different resonating group predictions of ref. [9]) (solid curve) and ref. [14]) (dot-dashed curve).

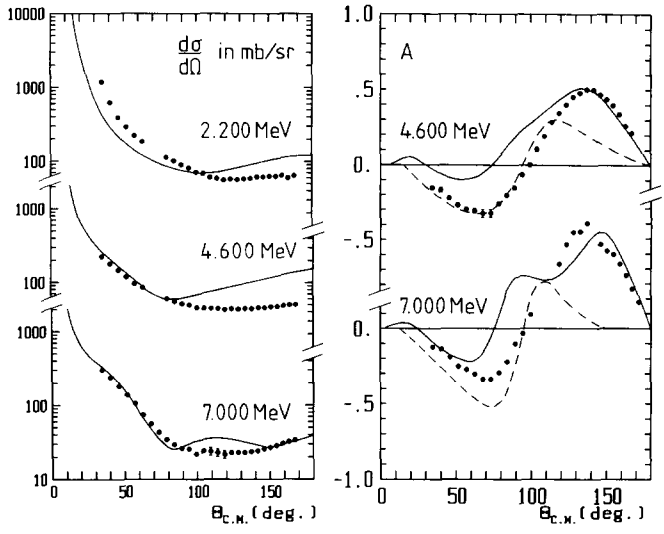

Fig. 12. ^{6}Li(p, p) data, compared with resonating group predictions of ref. [2]) for corresponding energies (2.26 MeV, 4.60 MeV and 6.93 MeV in the laboratory system). The dashed curves refer to a modified calculation with the $\frac{7}{2}^+$ channel being omitted.

While proton and neutron inelastic-scattering data agree very well, there are again some discrepancies to the theoretical predictions especially in the backward angular region.

6. Discussion

In fig. 1 the resonance levels obtained in our analysis are compared with an experimental level scheme [16]) and with the predictions of resonating-group calcula-

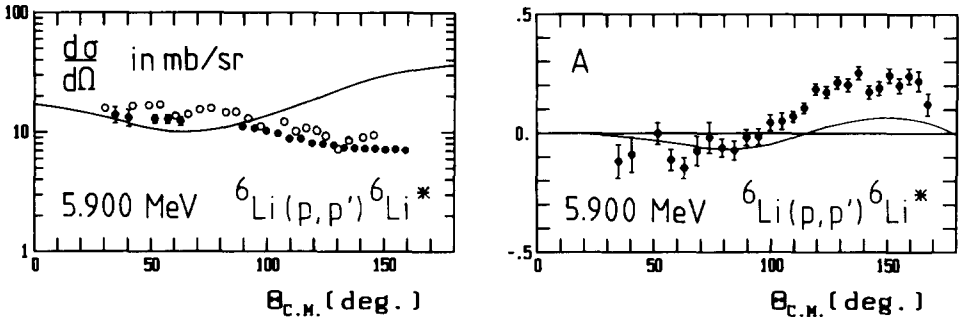

Fig. 13. Differential cross section and analyzing-power data of the inelastic scattering ^{6}Li(p, p')^{6}Li* (E_x = 2.183 MeV) at E_{lab} = 5.9 MeV (full circles). They are compared with corresponding predictions of ref. [2]) for $E_{c.m.}$ = 5.94 MeV and with corresponding inelastic neutron scattering data [15]), quoted in ref. [2]) (open circles).

tions of ref. [2]). The two $\frac{1}{2}^-$ levels and the $\frac{5}{2}^-$ level compare well with the corresponding levels in the theoretical predictions whereas the $\frac{3}{2}^-$ level is shifted to higher energies. The deduced resonance parameters are listed in table 2. The reduced widths γ_p^2 shown in the last column are defined according to Lane, Thomas [17]):

$$\Gamma_{\lambda L} = 2\gamma_{\lambda L}^2 P_L$$

where $\Gamma_{\lambda L}$ denotes the partial decay width via the elastic proton channel $\lambda = p$ and P_L is the penetrability through the Coulomb and angular momentum barrier (for simplicity the angular momentum index L is omitted in the table 2). The experimentally well-known level at E_x = 7.21 MeV (i.e. 1.6 MeV c.m. energy) appears in the excitation functions of the cross section (see the preceding paper). The phase-shift analysis is consistent with the assumed $J^\pi = \frac{5}{2}^-$ and with the resonance parameters of ref. [11]). Due to the ambiguities of the phase shifts a definite J^π assignment and determination of the partial width requires a larger analyzing-power data base in the proton energy range below 2.8 MeV.

The E_x = 9.9 MeV level has been assigned previously to $J^\pi = \frac{3}{2}^-$ by Legendre polynomial analyses of differential cross-section data for inelastic proton scattering on ^{6}Li to the first excited state at E_x = 2.19 MeV yielding $J^\pi = \frac{3}{2}^-$ or $\frac{5}{2}^-$ (ref. [18])) and to the second excited state at E_x = 3.56 MeV yielding $J^\pi = \frac{1}{2}^-$ or $\frac{3}{2}^-$ (ref. [19])). The result of our analysis was that this level is a superposition of three overlapping broad resonances with $J^\pi = \frac{1}{2}^-$ and $\frac{5}{2}^-$ which could be disentangled only by a phase-shift analysis of differential cross section and analyzing power.

We wish to express our thank to Prof. H.M. Hofmann and Dr. M. Herman for valuable discussions and for sending us the results of their resonating-group calculations prior to publication.

References

1) H.M. Hofmann, Nucl. Phys. **A416** (1984) 363c
2) H.M. Hofmann, T. Mertelmeier and W. Zahn, Nucl. Phys. **A410** (1983) 208
3) C. Petitjean, L. Brown and R.G. Seyler, Nucl. Phys. **A129** (1969) 209
4) W.D. Harrison and A.B. Whitehead, Phys. Rev. **132** (1963) 2607
5) R.G. Seyler, Nucl. Phys. **A124** (1969) 253
6) J.M. Blatt and L.C. Biedenharn, Rev. Mod. Phys. **24** (1952) 258; Phys. Rev. **86** (1952) 399
7) B.J.-R. Jenny, dissertation, Zürich, 1977
8) P.A. Schmelzbach, W. Grüebler, R.E. White, V. König, R. Risler and P. Marmier, Nucl. Phys. **A197** (1972) 273
9) H.G. Pfütner, Auli Li, K. Murphy, C.R. Howell, M.L. Roberts, I. Slaus, R.L. Walter, M. Herman and H.M. Hofmann, Proc. VIth Int. Symp. on polarization phenomena in nuclear physics, Osaka, 1985, p. 3;
M. Herman, Warshaw, private communication, 1985
10) L. Veeser and W. Haeberli, Nucl. Phys. **A115** (1968) 172
11) J.A. McCray, Phys. Rev. **130** (1963) 2034
12) C. Petitjean, L. Brown and R.G. Seyler, Nucl. Phys. **A129** (1969) 209
13) R.L. Walter *et al.*, Annual Report—TUNL XXVI, 1987, p. 91
14) H.M. Hofmann, Erlangen, private communication, 1985
15) H.H. Hogue, P.L. von Behren, D.W. Glasgow, S.G. Glendinning, P.W. Lizowski, C.E. Nelson, F.O. Purser, W. Tornow, C.R. Gould and L.W. Seagondollar, Nucl. Sci. Eng. **69** (1979) 22
16) F. Ajzenberg-Selove, Nucl. Phys. **A320** (1979) 1
17) A.M. Lane and R.G. Thomas, Rev. Mod. Phys. **30** (1958) 257
18) W.D. Harrison, Nucl. Phys. **A92** (1967) 253
19) W.D. Harrison, Nucl. Phys. **A92** (1967) 260